Supporting Online Material

Thermal Structure and Dynamics of Saturn's Northern Springtime Disturbance

L.N. Fletcher et al.

Materials and Methods

This article combined several infrared datasets to study the vertical properties of Saturn's northern springtime storm. Spectroscopic observations of Saturn's northern hemisphere at 0.5 and 2.5 cm^{-1} spectral resolution were provided by the Cassini Composite Infrared Spectrometer (CIRS, *17*). These were supplemented with narrow-band filtered imaging from the ESO Very Large Telescope VISIR instrument (*16*) to provide a global spatial context for the Cassini spectroscopy. Finally, nightside imaging from the Cassini Visual and Infrared Mapping Spectrometer (VIMS, *22*) provided a glimpse of the undulating cloud activity in the eastern branch of the disturbance. Each of these datasets, and the methods used to reduce and analyse them, will be described in detail below.

Spatial maps of atmospheric temperatures, aerosol opacity and gaseous distributions are derived from infrared spectroscopy using a suite of radiative transfer and optimal estimation retrieval tools developed at the University of Oxford, known collectively as Nemesis (*23*). Synthetic spectra created from a reference atmospheric model for Saturn and appropriate sources of spectroscopic line data (*6, 24*) are convolved with the instrument function for each dataset. Atmospheric properties are then iteratively adjusted until the measurements are accurately reproduced with physically-realistic temperatures, compositions and cloud opacities.

VLT/VISIR Thermal Imaging (7-20 μm):

Thermal images of Saturn were obtained at 7.9, 8.6, 9.0, 10.7, 12.3, 17.6, 18.7 and 19.5 μm on January 19th 2011 between 07:35-08:30 UT (Table S1), using the UT3 telescope at Cerro Paranal in Chile (Fig. S1). Program 386.C-0096(A) had been awarded time to study Saturn's slow seasonal evolution, but ESO granted our request to obtain these images of Saturn's storm as soon as the planet became available after solar conjunction. The images benefitted from a low water vapour humidity (<10%) and stable seeing on the night of the observations. The ESO data pipeline was used for initial reduction and bad-pixel removal via its front-end interface, GASGANO (version 2.3.0). An idealized wavelength-dependent point spread function representing the effects of diffraction and seeing was deconvolved from each image using the PIXON image reconstruction algorithm (*25*). Images were geometrically registered, cylindrically reprojected and absolutely calibrated using the techniques developed by Fletcher et al. (*26*). Radiometric calibration was achieved by scaling the observations to match Cassini/CIRS observations during a similar epoch.

The images were stacked to form a rudimentary 8-point image cube, and used to retrieve the tropospheric and stratospheric temperatures in two directions: north-south (using radiances within 10° longitude of the central meridian for each filter, centred on the disturbance) and east-west (taking a mean of measurements between 32-42°N, the central planetocentric latitudes of the disturbance). The latter was presented in Fig. 1, and shows the thermal contrasts associated with the storm head, centre and easterly branches.

At the central latitude of the disturbance (41°N), one degree of longitude is equivalent to approximately 780 km, allowing us to place the 10,000 km scale on Fig. 1B. Although the initial convective disturbance may have been mesoscale in extent (i.e., smaller than Saturn's deformation radius of ~1000 km), the storm grew to be synoptic in size to cover almost a third of the longitude circle (approximately 100,000 km). Of particular interest is the prominent cold oval shown in Fig. 1. From map projections of the VISIR imaging and T. Barry's visible observation (obtained from the International Outer Planet Watch Planetary Virtual Observatory and Laboratory, www.pvol.ehu.es), we find this vortex to be centred at 35.5°N (planetocentric latitude, or 41.2°N planetographic) and 314°W. It extends over 5±1° latitude and 7±1° longitude, being slightly broader in the visible maps than the thermal maps, although this could simply be a result of the differing contrasts between the visible and thermal data. All latitudes in the manuscript were fitted in planetocentric coordinates and converted to planetographic coordinates for retrieval. Although the vortex centre is consistent between the thermal and visible maps, there are differences in location between the albedo and thermal features in the eastern turbulent region in Fig. 1B/C, but these appear to be genuine offsets rather than mapping errors. Errors could still exist due to the differences in pixel scales and resolution between the two datasets, and the problem of limb darkening when fitting the exact location and size of the planet on the array. Nevertheless, we found consistency between three independent fitting techniques to within 0.5 degrees for all features.

VLT observed the storm longitudes again on January 27th, 31st and February 8th, but higher water vapour content produced a degraded quality with respect to the first image set. These demonstrated the continued presence of the hot stratospheric beacons and their westerly propagation (i.e., near stationary with respect to the underlying disturbance), and will be presented in a future publication.

Wavelength	*Time (UT)*	*Central Meridian*	*Sensitivity*
8.6	*07:44*	*290.1*	*Stratospheric CH_3D*
9.0	*07:49*	*292.9*	*Deep T(p), PH_3*
10.7	*07:56*	*296.9*	*Deep T(p), PH_3*
17.6	*08:02*	*300.2*	*H_2, 150 mbar T(p)*
18.7	*08:08*	*303.6*	*H_2, 200-mbar T(p)*
19.5	*08:15*	*307.6*	*H_2, 250-mbar T(p)*
12.3	*08:21*	*310.9*	*C_2H_6, 3-mbar T(p)*
7.9	*08:28*	*314.9*	*CH_4, 3-mbar T(p)*

Table S1: Thermal images obtained during the January 19th 2011 observing

sequence, showing the UT time of the observation, the central meridian longitude in System III west coordinates, and the primary parameter contributing to the radiance at each wavelength.

Cassini/CIRS Mid-Far Infrared Spectroscopy (7.4-200 μm)

Cassini/CIRS *(17)* is a Fourier Transform spectrometer with focal planes covering the far-infrared (10-600 cm^{-1}) and the mid-infrared (600-1400 cm^{-1}). Latitude scans of the northern hemisphere had been preplanned for late 2010 and early 2011 well in advance of the disturbance, so coverage of the storm at the same time as the VLT observations was fortuitous. Figs. 2-3 in the main article use retrieved atmospheric properties from the 50-1350 cm^{-1} spectral range (7.4-200 μm). The coverage of the datasets is shown in Fig. S2, demonstrating that these observations were not designed to provide global maps of Saturn, but were able to identify the key features of the disturbance. Two categories of observations were used:

1. Sit-and-stare observations (COMPSIT, Fig. S2B) with focal planes oriented north-south to capture the entire longitude circle at 45-55°N as Saturn rotated on January 2nd, 2011 (12:00-23:59 UT). The data were acquired at the highest apodized spectral resolution of CIRS, 0.5 cm^{-1}, and were utilized in Fig. 3 and S5.
2. Shift-and-stare observations (MIRTMAP) at 2.5 cm^{-1}, stepping southward in latitude and integrating for approximately 2 hours at each location. Identical observations in October 2010 (Fig. S2A, 06:00 UT October 22nd to 10:29 UT October 23rd) and January 2011 (18:30 UT January 19th to 17:29 UT January 20th, Fig. S2C) allowed us to measure the thermal anomalies associated with the disturbance.

The two categories provide different constraints on the characteristics of the storm – the high-resolution COMPSIT data permit accurate compositional retrievals but for a single latitude (e.g., Fig. 3 of the main text and Fig. S5), whereas the low-resolution MIRTMAPs cover a wider range of latitudes and allow us to retrieve thermal maps. Fig. S2 shows that the stratospheric hot spots evident in the ground-based imaging are also detected spectroscopically by CIRS (from an average of the 1290-1310 cm^{-1} region, centred on the ν_4 band of CH_4). Furthermore, because CIRS covers the whole latitude circle, we were better able to constrain the width of the stratospheric beacons on January 19th 2011, and show that the spatial variability of the emission (particularly the central vortex and stratospheric hotspots) in Figs. 1 and S2 are collocated between the ground-based and space-based instruments. This allows us to rule out spurious instrumental variations during the 20-hour CIRS observations.

The storm-induced thermal anomalies in the north-south and east-west directions (Fig. S3, S4) were retrieved from the mid-IR focal planes (2.5 cm^{-1} data) using the collision-induced H_2-He continuum between 600-680 cm^{-1} for tropospheric temperatures (70-300 mbar) and CH_4 emission between 1250-1350 cm^{-1} for stratospheric temperatures (0.5-5.0 mbar, using techniques described by *(6, 27)*). Spectra were binned on a 5° latitude grid (stepped every 2.5°) and a 10° longitude grid (stepped every 5°). The longitudinal plots

(Fig. 2 of the main article) used data from 25, 35 and 45°N as displayed in Fig. S2. The temperature profiles were used to derive stratospheric C_2H_6 and C_2H_2 abundances using the 700-850 cm^{-1} range of the same data. The longitudinal variation of tropospheric PH_3 could not be measured from the mid-IR using such fine-scale gridding due to signal-to-noise constraints in the 1100-1200 cm^{-1} region, so we had to turn to the 50-150 cm^{-1} CIRS spectra to study this atmospheric tracer.

The lapse rate (*dT/dz*) in Fig. S3 and S4 was estimated from the thermal profiles before and after the storm onset to demonstrate that the tropospheric cooling increased *dT/dz* over the storm, and therefore decreased the atmospheric stability to convection. The change is significant when compared to the dry adiabatic lapse rate ($g/c_p \sim 1$ K/km, where g is the gravitational acceleration and c_p the specific heat capacity). Saturn's atmosphere approaches this dry adiabatic lapse rate in the deep atmosphere, but has a smaller lapse rate in the stably-stratified upper troposphere (*27)* due to radiative heating which leads to a temperature inversion at the tropopause. Systematic errors from smoothing in the retrieval process contribute considerable uncertainty to the estimate of *dT/dz*, but retrieval errors should contribute equally to the October 22nd and January 19th datasets so that the difference between the measured lapse rates is a robust quantity.

The longitudinal PH_3 distribution at 50°N in Fig. 3 (main article) was derived from the January 2nd longitude scan at 0.5 cm^{-1}. Tropospheric temperatures (80-800 mbar) and para-H_2 were measured from the 150-500 cm^{-1} collision-induced continuum (*27*), and then used to fit the far-IR rotational lines of PH_3 and NH_3 between 50-150 cm^{-1}. Although the far-IR focal plane has a lower spatial resolution than the mid-IR focal plane (*17*), longitudinal variability of PH_3 was measured at the northern edge of the storm. Furthermore, tropospheric and stratospheric temperatures derived from the mid-IR focal planes on January 2nd at the storm's northern edge (Fig. S5) feature similar thermal contrasts to those from the January 19th data, albeit with a smaller magnitude as they are further from the central latitude of the storm (40°N).

The vertical profile of PH_3 was defined by a deep mole fraction for pressures exceeding 550 mbar and a decreasing abundance with height (*21*). For the purposes of this study, we simply scaled this profile to fit the rotational features. However, retrieved PH_3 from the far-IR rotational lines (50-150 cm^{-1}) is significantly larger than that from vibrational lines near the 9-μm dyad and the 5-μm pentad polyad. This discrepancy is the source of ongoing investigations (see *(21)* for a full discussion), but the *relative* PH_3 variation derived from the 50°N scan appears to be robust.

Cassini/VIMS Near-IR Spectroscopy (4.5-5.1 μm):

Cassini/VIMS (*22*) fortuitously acquired imaging of the southern branch of the disturbance, far to the east of the main storm core, during a mapping sequence focused on Saturn's equatorial plumes on January 9th, 2011. The images were obtained on Saturn's nightside, so that the effects of reflected sunlight could be neglected in modeling of the 4.6-5.1 μm thermal emission spectrum. The image cube covered a small longitude range

between 165-200°W with a spectral resolution of 15 nm. The morphology of VIMS spectra in this range is determined by tropospheric PH_3 and aerosol opacity, with small perturbations from NH_3 and AsH_3. We use a model for the vertical cloud structure (*24*) consisting of two opacity sources – a deep cloud (τ_1) at 2.8-bar and an upper cloud (τ_2) at 1.4 bar. Such a configuration has been found to produce an excellent fit to nadir VIMS spectra under both scattering and non-scattering assumptions, although the solution is non-unique and highly sensitive to the optical properties of the aerosol particles, which are presently unknown. We retrieve the optical depth of each of these clouds, as well as scaling well-mixed abundances of PH_3, NH_3 and AsH_3, to obtain a good fit to the data. Both scattering and non-scattering retrievals were performed, with negligible differences in the quality of the fits.

Given the extent of the degeneracies inherent in modeling VIMS spectra in the 4.6-5.1 μm region (*24*), we selected data in two latitude regions (30°N and 22°N), one covering the wave-induced storm clouds and the other representing a quiescent region of Saturn's troposphere. The *relative* properties of the two latitude circles are compared in Fig. 4 of the main article.

Zonal and Meridional Velocities

The primitive equations of atmospheric motion (e.g., *28*) can be used to relate the vertical temperature structure to the zonal, meridional and vertical velocity fields. Zonal winds are calculated assuming geostrophic balance between meridional pressure gradients and Coriolis forces. In log-pressure coordinates, the thermal wind equation is:

$$f\frac{\partial u}{\partial \ln(p)} = -\frac{R}{a}\frac{\partial T}{\partial \theta}$$

where f is the Coriolis parameter $f=2\Omega \sin\theta$ (where Ω is the planetary angular velocity, θ is the latitude), a is the mean planetary radius, u is the zonal (eastwards) velocity and R is the molar gas constant divided by the mean molar weight of Saturn's atmosphere. Geostrophy is accomplished within storm features as the Rossby number ($Ro=U/fL$) is small (0.03) for the characteristic velocities (u=25 m/s for this zonal jet) and length scales (L~5000 km for the new oval and storm head) encountered within the disturbance, although ageostrophic effects cannot be entirely ruled out. Saturn's zonal velocity profile at the cloud-tops, u (*15*), was determined by tracking visible cloud features, although the precise altitude of these tracers is subject to considerable uncertainty. We calculate the vertical windshear for the two 2.5 cm^{-1} CIRS observations in Fig. S2, then integrate the thermal wind equation vertically, using the zonal winds placed at 500 mbar, to estimate the vertical variations of the zonal windspeeds. The difference between zonal winds on October 22nd and January 19th are shown in Fig. 2C of the main article, revealing the storm-induced modifications of high-altitude zonal jets.

A similar geostrophic balance occurs between meridional windshear and the east-west temperature gradients (Fig. S4), and suggest that the existence of thermal perturbations could cause the zonal jets to meander in latitude as they do on Earth, and possibly form closed vortices such as those observed in Fig. 1.

Vertical Displacements

The thermodynamic energy equation provides a diagnostic balance between vertical advection (leading to adiabatic heating or cooling of the atmosphere) and the relaxation of the atmosphere to an equilibrium temperature profile by radiative heating and cooling. The thermodynamic energy, or heat equation (*28*), can be expressed as;

$$\frac{DT}{Dt} + \frac{RT}{Hc_p}w = \frac{Q}{\rho c_p} \approx \frac{T_e - T}{\tau_R}$$

where *DT/Dt* is the advective derivative of temperature, *H* is the atmospheric scale height, c_p is the specific heat capacity of Saturn's atmosphere with density ρ, calculated assuming a simple H_2-He-CH_4 atmosphere and a thermal equilibrium para-hydrogen fraction. Q is the net diabatic heating of the atmosphere, T_e - T is the perturbation of the atmosphere away from the radiative equilibrium profile, T_e, and τ_R is the radiative relaxation time. We expand the advective derivative and retain only the vertical motion terms in *w*:

$$\frac{\partial T}{\partial t} + w\left(\frac{\partial T}{\partial z} + \frac{RT}{Hc_p}\right) = \frac{Q}{\rho c_p} \approx \frac{T_e - T}{\tau_R}$$

The partial derivative of temperature with altitude is the atmospheric lapse rate, Γ. Saturn's radiative relaxation time in the ambient atmosphere is long (10 years near the tropopause), so 45 days is insufficient time for the atmosphere to relax to perturbations of one scale height or greater, so we can assume the term on the right hand side is vanishingly small and that the dominant balance is between the temporal evolution of the temperature field and the advective term:

$$\frac{\partial T}{\partial t} + w\left(\Gamma + \frac{RT}{Hc_p}\right) \approx 0$$

For vertical motions that are smaller than a scale height, *H*, we can relate the observed thermal contrasts to the vertical displacements to produce Fig. 2D.

$$\Delta z \approx \Delta T / \left(\Gamma + \frac{RT}{Hc_p}\right)$$

The displacements estimated using this technique are rather crude, as we have not accounted for the possibilities of horizontal mixing or non-hydrostatic effects that may be at work within the convective structures. However, the observed temperature contrasts can be produced with vertical displacements of less than a scale height.

Finally, we were also able to use acetylene and phosphine as passive tracers of the atmospheric motions to obtain similar estimates of the displacement. This was done by estimating the vertical velocity using the continuity equation:

$$\frac{D\chi}{Dt} = \frac{\partial \chi}{\partial t} + w\frac{\partial \chi}{\partial z} = P - L$$

where χ is the mole fraction of interest, and the partial derivative with respect to altitude gives the vertical gradient of the species (estimated from retrievals at quiescent latitudes). If we assume no sources or sinks (i.e., production P and loss L are equal) so that the right hand side is zero, we can evaluate the expression for small displacements to estimate w and hence the vertical displacements.

Wave Phenomena

Numerical modeling of convective plumes on Saturn (*5, 18)* suggests that vigorous water storms can cause convective overshooting up to the 60-mbar level, 20 km above the tropopause. This strong convection could excite a broad spectrum of wave activity, which may be responsible for transporting energy and momentum into the stratosphere. The stratospheric perturbations cannot be from direct convection (as potential temperature is conserved in adiabatic ascent/descent, the size of the tropospheric temperature perturbation would be enormous), but must be a stratospheric response to the deeper convective forcing. If the stratospheric perturbations are a manifestation of a large wave of some sort, then the dimensions can be estimated from the thermal maps: we estimate the vertical wavelength to be approximately 320 km using the distance between the tropopause and the 2-mbar level of the stratospheric beacons, yielding a vertical wavenumber m=2.0x10^{-5} m^{-1}. The horizontal wavelength was measured from the CIRS data to be approximately 120° longitude (93600 km), giving a horizontal wavenumber of k=6.7x10^{-8} m^{-1}. Further observations of the stratospheric beacons must be acquired to chararacterise the evolution of these features and the nature of the wave activity.

Supporting Figures

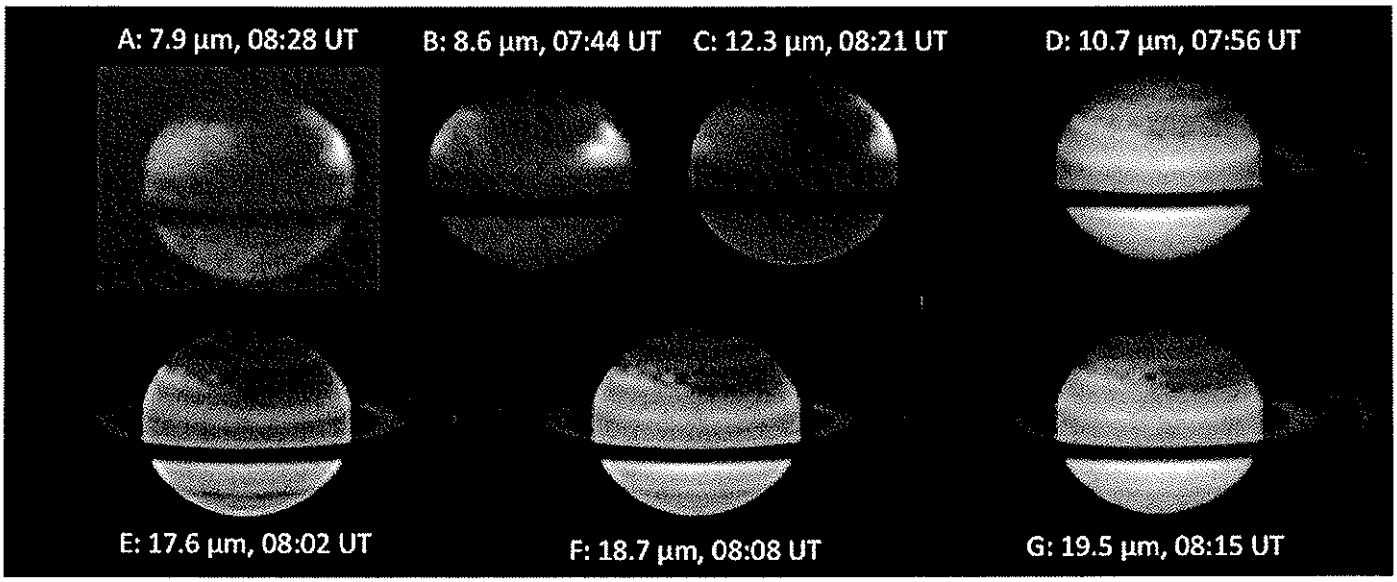

Figure S1. Montage of VLT Thermal Imaging from January 19th 2011. Frames A-C show stratospheric emission from methane and ethane primarily sensitive to temperatures in the 1-20 mbar region. The image at 10.7 μm (D) is sensitive to a combination of 500-mbar temperatures and tropospheric PH_3. Frames E-G are sensitive to Saturn's collision-induced H_2-He continuum and probe temperatures between 100-300 mbar.

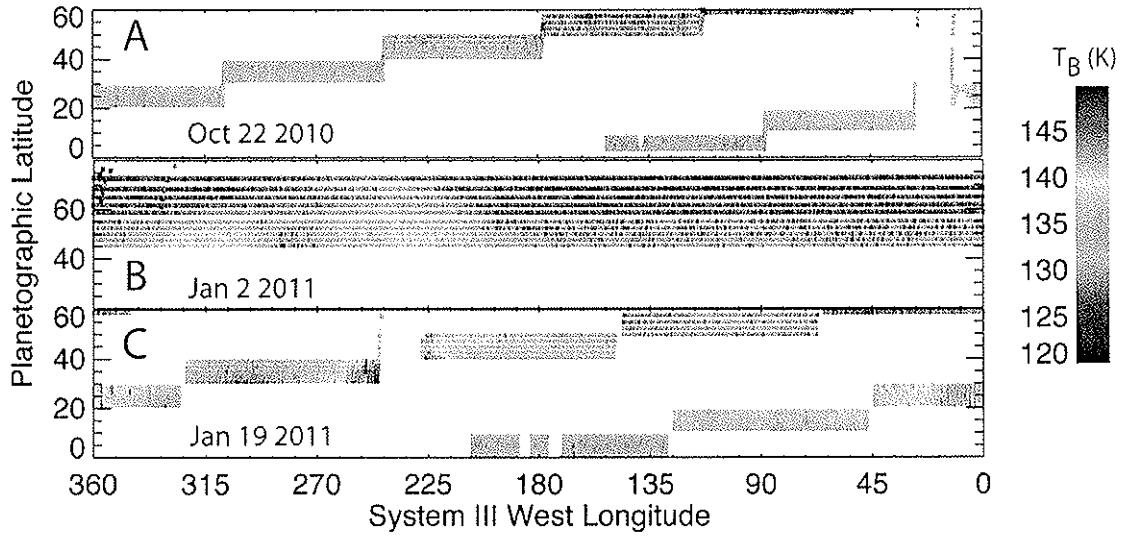

Figure S2. Cassini/CIRS spatial coverage of the northern disturbance. The quiescent state of Saturn's stratosphere is shown in A, where the radiance in the 1290-1310 cm^{-1} region has been averaged and converted to brightness temperatures for each pixel. Panels

A and C were acquired at 2.5 cm^{-1} spectral resolution using a step-and-scan technique, moving the focal planes southward towards the equator. Panel A was acquired before the onset of the disturbance on October 22nd, 2010; panel C was acquired during the mature phase of the disturbance on January 19th 2011. Panel B was acquired using a sit-and-stare technique at 0.5 cm^{-1} spectral resolution, and shows the stratospheric perturbations at the northern edge of the disturbance on January 2nd 2011. CIRS radiance maps are subject to both random errors and systematic noise (e.g., electrical interference creating spikes in the interferograms), which can lead to the noisy appearance of these maps (particularly in C).

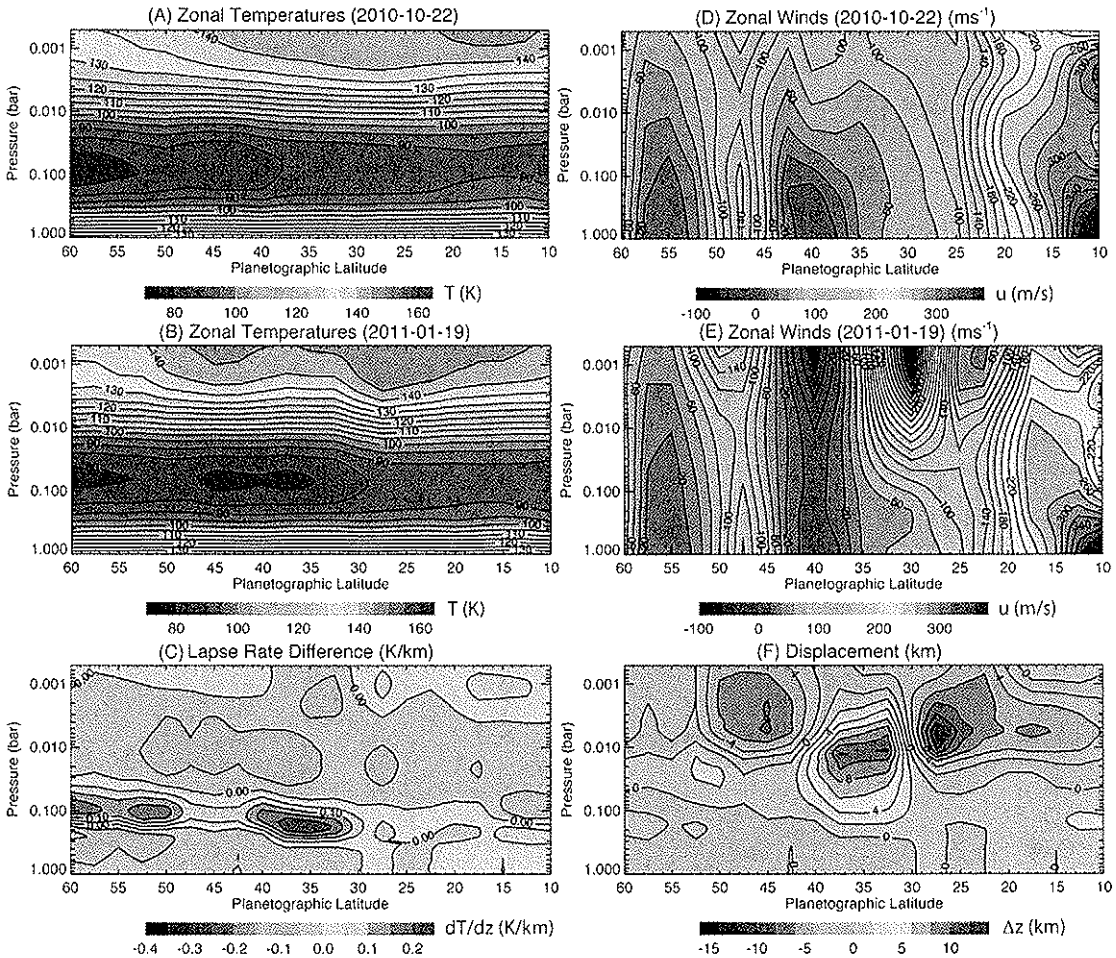

Figure S3. North-South Zonal temperature variability derived from Cassini/CIRS observations. Vertical temperature profiles were calculated at a range of latitudes between 10-60°N using the 600-680 cm^{-1} tropospheric continuum and stratospheric emission in the 1250-1350 cm^{-1} region. The vertical lapse rate, -dT/dz, was estimated from the temperature profiles, and the difference is displayed in C. Zonal winds (D, E) were estimated using the thermal windshear equation, integrating cloud-tracked zonal winds (S13) above the 500-mbar pressure levels. The difference between the zonal temperature retrievals in A and B were used to estimate the vertical displacements in F.

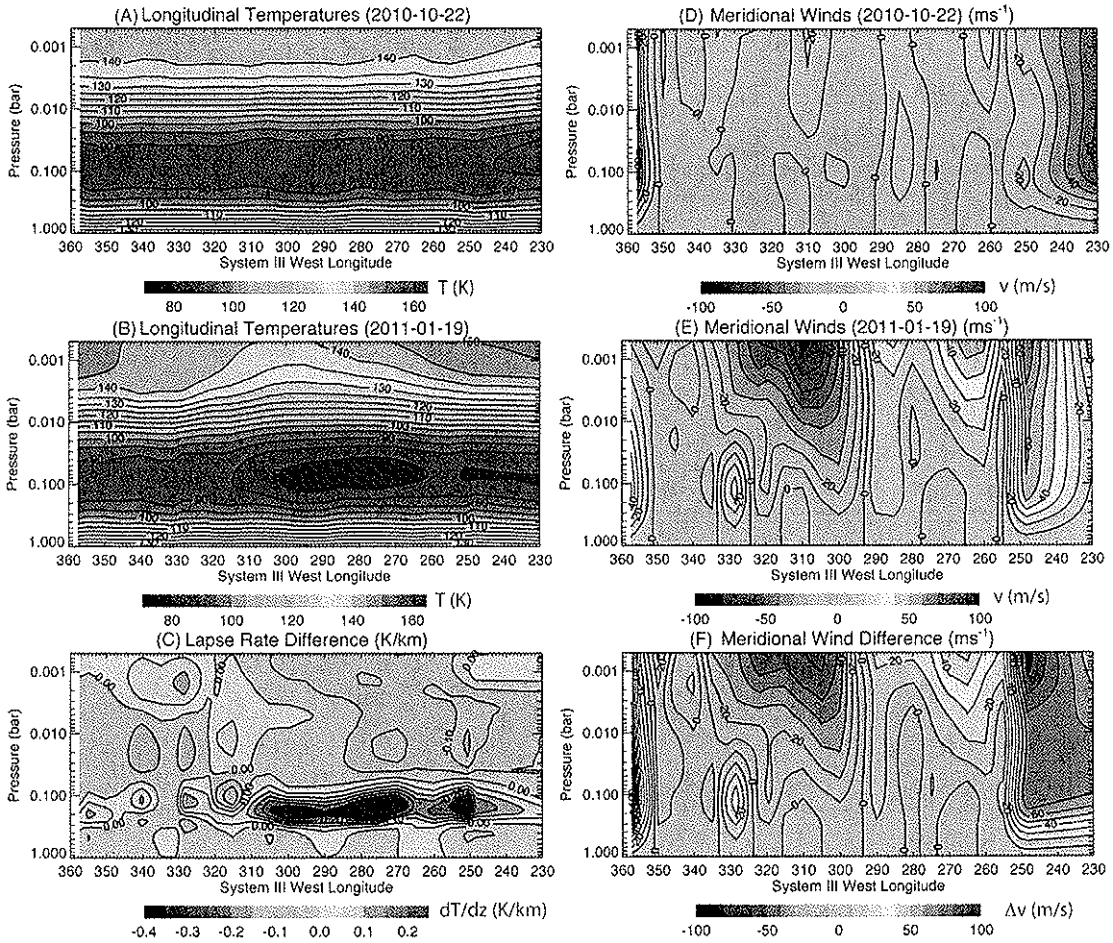

Figure S4. Longitudinal temperature profiles derived from Cassini/CIRS observations. We use the same methods described in Fig. S3 to derive the vertical temperature structure at a range of longitudes (A, B), and the difference in atmospheric lapse rate over the upwelling branch of the disturbance (C). The thermal windshear equation is used to determine the vertical shear on meridional winds (dv/dz) from the longitudinal thermal gradients (dT/dx), which is then integrated in the vertical (assuming zero meridional motion at 1 bar) to show the vertical variations of meridional winds (v) in D and E. The windshear acts to damp any clockwise motion (i.e., anticyclonic motion) generated by the storm. The differences between pre- and post-onset meridional winds is shown in F. These meridional winds could create closed vortices within the disturbance, and may cause the zonal jets to meander in latitude as they do on the Earth.

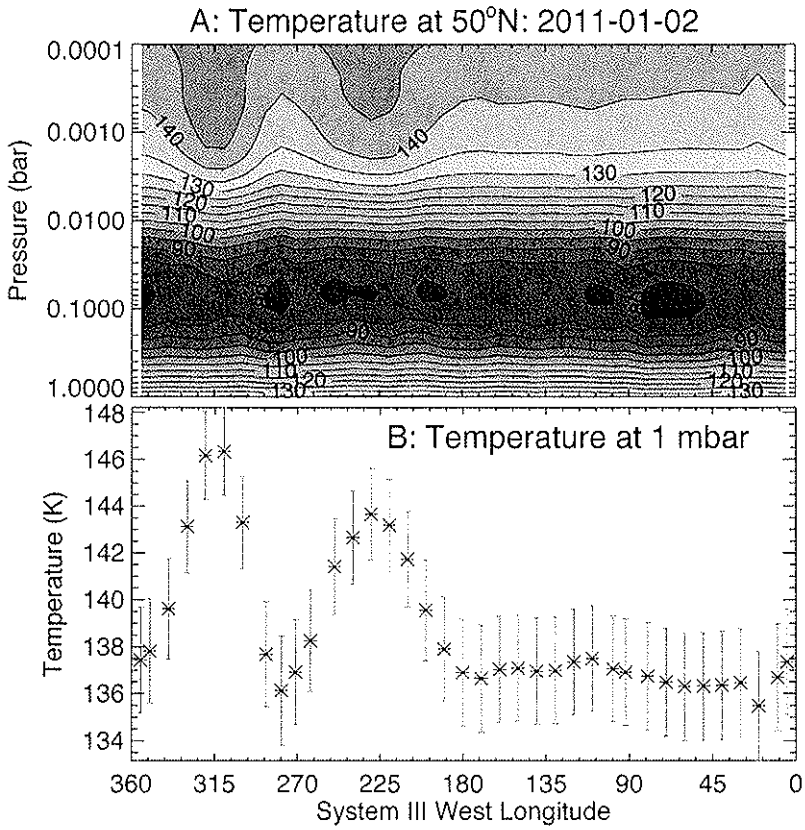

Fig. S5: Temperatures retrieved from Cassini/CIRS 0.5 cm^{-1} COMPSIT observations at the northern edge of the storm. The two stratospheric beacons were first detected in CIRS observations on January 2nd 2011, 10° north of the central storm latitude. The tropospheric cooling is not as evident here as at 40°N (consistent with the morphology displayed in Fig. 1 of the main article).

Supporting References

S1. Flasar, F. M. et al. Exploring The Saturn System In The Thermal Infrared: The Composite Infrared Spectrometer. Space Science Reviews 115, 169–297 (2004).

S2. Lagage, P. O. et al. Successful Commissioning of VISIR: The Mid- Infrared VLT Instrument. The Messenger 117, 12–16 (2004).

S3. Brown, R. H. et al. The Cassini Visual And Infrared Mapping Spectrometer (Vims) Investigation. Space Science Reviews 115, 111–168 (2004).

S4. Irwin, P. et al. The NEMESIS planetary atmosphere radiative transfer and retrieval tool. Journal of Quantitative Spectroscopy and Radiative Transfer 109, 1136–1150 (2008).

S5. Fletcher, L. N. et al. Seasonal change on Saturn from Cassini/CIRS observations, 2004-2009. Icarus 208, 337–352 (2010).

S6. Fletcher, L. N. et al. Saturn's Zonal Ammonia and Cloud Distributions from

Cassini/VIMS 4.5-5.1 μm Nightside Spectroscopy. Icarus, submitted (2011).
S7. Puetter, R. C. & Yahil, A. The Pixon Method of Image Reconstruction. In Mehringer, D. M., Plante, R. L. & Roberts, D. A. (eds.) ASP Conf. Ser. 172: Astronomical Data Analysis Software and Systems VIII, 307–316 (1999).
S8. Fletcher, L. N. et al. Retrievals of atmospheric variables on the gas giants from ground-based mid-infrared imaging. Icarus 200, 154–175 (2009).
S9. Fletcher, L. N. et al. Characterising Saturn's Vertical Temperature Structure from Cassini/CIRS. Icarus 189, 457–478 (2007).
S10. Fletcher, L. N., Orton, G. S., Teanby, N. A. & Irwin, P. G. J. Phosphine on Jupiter and Saturn from Cassini/CIRS. Icarus 202, 543–564 (2009).
S11. Baines, K. H. et al. Saturn's north polar cyclone and hexagon at depth revealed by Cassini/VIMS. Plan. & Space Sci. 57, 1671–1681 (2009).
S12. Holton, J.R., An Introduction to Dynamic Meteorology, Academic Press (2004).
S13. Sanchez-Lavega, A., Rojas, J. F. & Sada, P. V. Saturn's Zonal Winds at Cloud Level. Icarus 147, 405–420 (2000).
S14. Conrath, B. J., Gierasch, P. J. & Leroy, S. S. Temperature and circulation in the stratosphere of the outer planets. Icarus 83, 255–281 (1990).